Optimal exciting motion for fast robot identification. Application to contact painting tasks with estimated external forces

Takuma Katsumata, Benjamin Navarro, Vincent V. Bonnet, Philippe Fraisse, André Crosnier, Gentiane Venture

Version of Record: https://www.sciencedirect.com/science/article/pii/S0921889017307091
Manuscript_2781545f6360c9fb38f9273ac3d2ee87

Optimal exciting motion for fast robot identification. Application to contact painting tasks with estimated external forces.

Takuma Katsumata, Benjamin Navaro, Vincent Bonnet, Philippe Fraisse, André Crosnier, and Gentiane Venture

***Abstract*—Accurate geometric and inertial parameter estimates of a modern manipulator are of crucial importance to obtain good performances during a contact task or for obtaining more and more required realistic simulations. CAD data are often provided by the manufacturer, but these are inaccurate and do not take into account eventual end-effector modifications. Fortunately, they can be identified. However, in real industrial applications, dynamic identification is rarely performed because it supposedly requires a cumbersome and long procedure. There is a need of a practical but accurate method to identify dynamics parameters. Thus, this paper proposes a practical framework to identify a Kuka LWR robot in less than 10 s. An experimental comparison between several cost functions showed that $\log\{\det(\cdot)\}$ is the best trade-off for getting a good parameters accuracy within a minimal time. The procedure identifies very accurately the inertial parameters of the robot and of its end-effector and recognizes its geometric parameters from a look-up table. When using identified parameters, joint torques were estimated with an RMS difference lower than 1 N.m when compared to measured ones. The identified model was then used to generate a contact painting trajectory. During this contact task, the external forces were estimated and controlled without the use of a force sensor. Experimentation showed that the external forces could be identified with an RMS difference lower than 3 N.**

***Index Terms*—Dynamic identification, force control, painting task, Kuka LWR.**

I. Introduction

MODERN robotics is highly linked to the development of new applications involving human-robot physical interactions in unknown environments. For those, an efficient dynamics controller, force or torque controller, is of crucial importance [1]. Dynamics controllers are often based on the dynamics model of the robot. To perform correctly, such controllers require an accurate estimate of segments inertial parameters (SIP). SIP refer to the mass, the 3D center of mass (CoM) and the six elements of the inertia matrix of each segment of a mechanical structure. In robotics, SIP are usually extracted from CAD data. However, CAD data do not take into account cabling, covers, glued components, or the several, sometimes daily, modifications of the end-effector of a multipurpose manipulator. This is why during the last decades, several groups have developed methods to identify the dynamics of all kinds of robots [2]–[10]. There are several ways to estimate the SIP of a manipulator. Least squares methods and maximum likelihood estimation methods are still the most popular approaches [11], [12]. Even if state observer [13] or adaptive filters [9], [14] can be used to estimate SIP online, it is preferable to use specially designed optimal exciting motion to improve the accuracy of an identification process [6], [8], [10], [12], [15], [16]. The last 20 years have seen the development of numerous approach aiming at facilitating the identification process of a robot by using exciting motions generated using constrained optimization processes. This allow to improve the quality of the identification process while minimizing the overall required time [15]. The literature studies use optimization to find the joint trajectories that minimize a criterion related to the condition number, the $\log\{\det(\cdot)\}$ or even the Hadamard's inequality [10]. However, it is not clear which cost function should be used to minimize the time required to perform an identification process. This is of importance since multi-tasks and reconfigurable robots, that need to be identified often, are more and more popular. Once the SIP are identified, advanced inverse dynamics control [18] can be used to control the interactions forces with the environment for example. Interactions forces are present in numerous industrial tasks and in the presence of uncertainties force control has a clear advantage over traditional position based controllers since more adaptable. Indeed, in the case of a position based approach, if the assignment or the robot end-effector tool is changed, costly new software implementation and/or a new layout of the robot surroundings are required. Thus, a force controlled approach could be more cost-effective in the long run. A force controller is usually based on a force sensor. The main drawbacks with using a force sensor is that it is expensive, fragile, it often requires calibration, and that it limits the robot's maximal payload. An alternative of using a force sensor would be to estimate the external forces applied to the robot based on sensing already available in the robot. Usually this includes joint position sensors and torques exerted by the motors. Methods for external forces estimation are also available in commercial industrial robot systems, such as provided by ABB [17]. The functioning principle of these systems are, unfortunately, often unknown and they are designed to correctly predict only very large external forces. Recently, several authors proposed to estimate external forces trough a state observer [13], introducing delay, or black box approaches [19], requiring a large amount of data. The latter are specific to each robot and can be cumbersome to use since the dynamics of the robot should be learned for different types of motions as the generalization is not guaranteed. State observers are also very sensitive to acceleration discontinuities that can cause transient behavior in the estimates of the

external forces [13]. Also, since the robot's inertial parameters are not separately identified, learning approaches are not convenient for simulation. An other common approach is to consider the residue between the measured joint torques and the estimated ones, from an identified model, as being an image of the external forces and moments [20]–[22]. However, to the best of our knowledge such approaches have never been validated in a real industrial dynamic contact task [21].
Consequently, in this paper, we proposed to use a model based approach since we believe that there is still possibilities for improvement. Mainly the identification could be performed more accurately and efficiently, in terms of required time, using specifically designed trajectories. Because the joint torques residue requires the robot's Jacobian matrix, the accuracy of external forces is also directly related to the accuracy of the kinematics. Wilson et al. [11] have proposed an interesting approach to estimate the kinematics, i.e the length, of a pendulum like tool from the inertial parameters estimation of the center of mass. However, this study was limited to a one degree-of-freedom model and to a unconstrained trajectory generation task.

A. Paper contribution

In this context, the paper proposes a practical study to determine very accurately the SIP of a serial manipulator in a short time (a few seconds). The goodness of the identification is demonstrated with a force control framework allowing to estimate external forces without force sensor, rather using solely an identified model, joint angles and joint torque sensors. Our approach is demonstrated with the popular KUKA LWR robot (KLWR) performing a painting task with a roller. Together with this paper is submitted to the community [23] the optimal exciting motion to be played onto the KLWR, the KLWR identification pipeline, the identified inertial parameters and the corresponding V-REP dynamics simulation. Beside that, the contributions of this paper are in order of importance:

- a comparison of different cost functions used to generate the best optimal exciting motion in the minimum amount of time,
- a new method to estimate the inertial and geometric parameters of an end-effector in industrial context,
- an improved method to estimate the external forces without force sensor based on dynamics identification results.

An overview of the framework is represented on Fig.1. The paper is organized following figure 1. In section II.A the KLWR geometric, dynamics and identification models are described. Section III presents the generation of optimal exciting motion and compares different optimality criterion. Section IV and V present the painting trajectory generation and its tracking with a classical position and force controller based on the identified models. Section VI presents the experimental results obtained with the KLWR and two types of rollers. Finally, the paper ends by discussing the advantages and limitations of the proposed framework.

II. KUKA LWR Model

A. DH table

The forward kinematics model of the KLWR was calculated from the modified Denavit-Hartenberg table (Table I). The KLWR is composed of N_L=8 rigid segments articulated by N_J=7 DoF (Fig. 2). The segment lengths L_1, L_2, L_3 were set using available CAD data [24], [25].

TABLE I
Modified DH parameters of the KUKA LWR

i	a_i	μ_i	σ_i	α_i	d_i	θ_i	r_i
1	0	1	0	0	0	θ_1	L_1
2	1	1	0	$\pi/2$	0	θ_2	0
3	2	1	0	$-\pi/2$	0	θ_3	L_2
4	3	1	0	$-\pi/2$	0	θ_4	0
5	4	1	0	$\pi/2$	0	θ_5	L_3
6	5	1	0	$\pi/2$	0	θ_6	0
7	6	1	0	$-\pi/2$	0	θ_7	0

B. Inverse geometric model

The calculation of the KLWR's inverse geometric model is not trivial since it has 7 DoF. This redundancy problem can be solved classically using the pseudo-inverse Jacobian matrix and its nullspace to avoid joint limitations, for example. However, in industrial context it is preferable to use an analytic and reliable solution. Consequently, the redundancy problem was addressed by fixing the KLWR's swivel angle, φ, similarly to Tolani et al. [26] and subsequently using the classical Paul method. With this approach, the elbow is still free to swivel about a circular arc whose normal vector is parallel to the axis defined from the shoulder to the wrist for any given end-effector pose. In Fig. 3, $\mathbf{P}_s$, $\mathbf{P}_e$, $\mathbf{P}_w$ define the position of the robot's shoulder, elbow and wrist, respectively. The origin of the coordinate system $\mathbf{P}_s$ is coincident with the shoulder location. To mathematically describe this circle, the normal vector $\hat{\mathbf{n}}$ of the plane formed by the unit vector in the direction from the shoulder to the wrist was defined. A local coordinate system was then created from the two unit vectors $\hat{\mathbf{u}}$ and $\hat{\mathbf{v}}$. Note that $\hat{\mathbf{u}}$ was arbitrarily set to be the projection of a user defined vector $\hat{\mathbf{b}}$. The mathematical descriptions of $\hat{\mathbf{u}}$, $\hat{\mathbf{v}}$, and $\hat{\mathbf{n}}$ vectors can be found in Tolani et al. [26]. The equation of the position of the elbow joint can be obtained from trivial trigonometry relations [26]:

$$\begin{aligned} \cos(\alpha) &= \frac{L_2^2 + D_{sw}^2 - L_3^2}{2L_2 D_{sw}} \\ \mathbf{c} &= \cos(\alpha) L_2 \hat{\mathbf{n}} \\ R &= \sin(\alpha) L_2 \\ \mathbf{P}_e(\varphi) &= \mathbf{c} + R(\cos(\varphi)\hat{\mathbf{u}} + \sin(\varphi)\hat{\mathbf{v}}) \end{aligned} \tag{1}$$

Finally, from the elbow position $\mathbf{P}_e$ and from the desired end-effector pose the recursive classical Paul method was used to solve the inverse geometric problem.

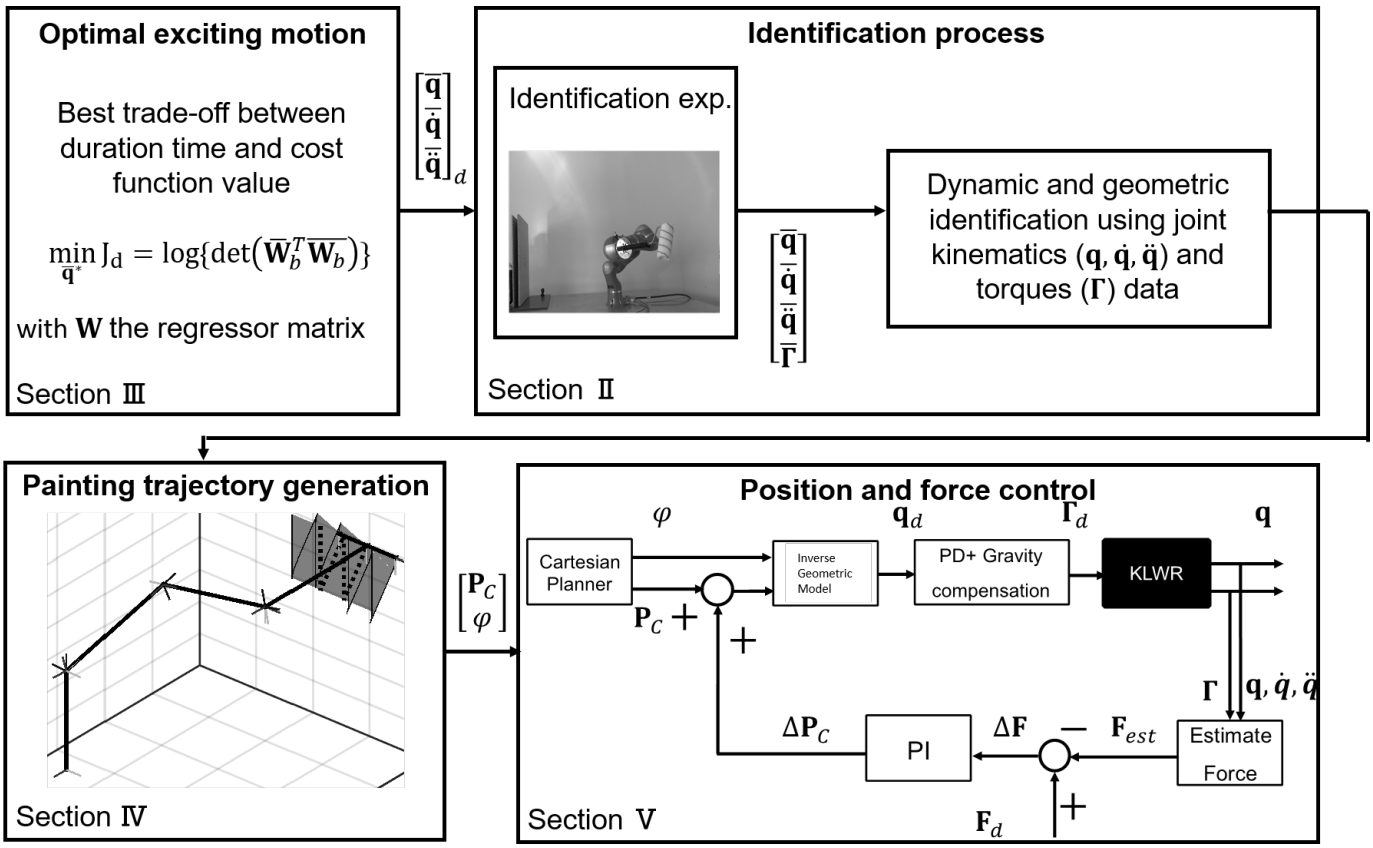

Fig. 1. Overview of the proposed framework. Optimal exciting motions are generated (first block) to excite the inertial parameters. Using the resultant trajectories, the inertial and geometric parameters are identified (second block). A painting trajectory is generated based on the updated models (third block) and tracked with a position and force controller able to estimate the external forces without force sensor.

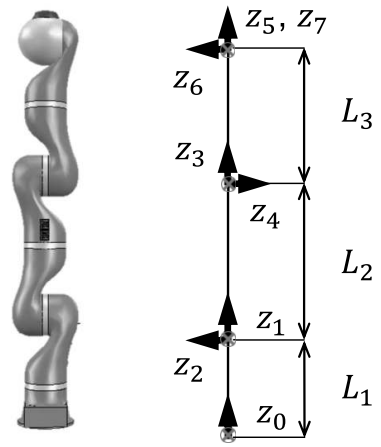

Fig. 2. Description of the KUKA LWR robot. Frames and segment definition used in the modified Denavit-Hartenberg description Table I.

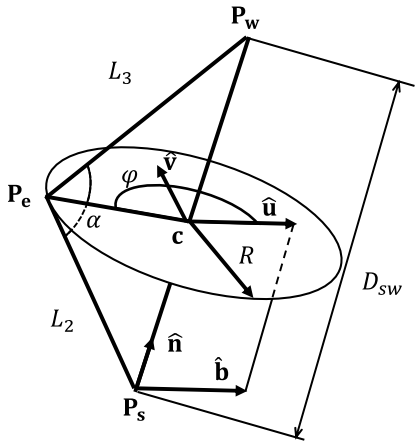

Fig. 3. The elbow joint is free to move on a circle for any pose of the end-effector.

C. Dynamics models

The inverse dynamics model of the KLWR was calculated from Newton-Euler equations to obtain the joint torques vector $\boldsymbol{\Gamma}$ ($N_J \times 1$) [27].

$$\begin{aligned} \boldsymbol{\Gamma} &= \mathbf{M}(\mathbf{q})\ddot{\mathbf{q}} + \mathbf{C}(\mathbf{q}, \dot{\mathbf{q}}) + \mathbf{G}(\mathbf{q}) + \boldsymbol{\Gamma}_f + \boldsymbol{\Gamma}_{ext} \\ \boldsymbol{\Gamma}_f &= \mathrm{diag}(\dot{\mathbf{q}})\mathbf{F}_v + \mathrm{diag}(\mathrm{sign}(\dot{\mathbf{q}}))\mathbf{F}_c \end{aligned} \tag{2}$$

where $\mathbf{q}$, $\dot{\mathbf{q}}$ and $\ddot{\mathbf{q}}$ are the $N_J \times 1$ vectors of joint angles, velocities and accelerations, $\mathbf{M}(\mathbf{q})$ $(N_J \times N_J)$ is the robot inertia matrix, $\mathbf{C}(\mathbf{q}, \dot{\mathbf{q}})$ $(N_J \times 1)$ is the vector of Coriolis and centrifugal terms, and $\mathbf{G}(\mathbf{q})$ $(N_J \times 1)$ is the vector of the gravitational terms. $\mathbf{\Gamma}_{ext}$ is the joint torques vector representing the influence of the external forces. $\mathbf{\Gamma}_f$ is the $N_J \times 1$ vector of joint torques due to coulomb and viscous friction effects. $\mathbf{FC} = [FC_1 ... FC_{N_J}]^T$ $(N_J \times 1)$ is the vector containing the Coulomb's friction coefficients and $\mathbf{FV} = [FV_1 ... FV_{N_J}]^T$ $(N_J \times 1)$ is the vector containing the viscous friction coefficients.

The equations of motion are linear with respect to the inertial parameters expressed in the joint frames [2]. Thanks to this property the observation matrix, also called regressor matrix, can be built and (2) then rewritten as:

$$\mathbf{W}(\mathbf{q}, \dot{\mathbf{q}}, \ddot{\mathbf{q}})\mathbf{\Phi} = \mathbf{\Gamma} \tag{3}$$

where $\mathbf{W}$ $(N_J \times (10N_L + 2N_J))$ is the regressor of the chains and $\mathbf{\Phi}$ $((10N_L + 2N_J) \times 1)$ is the vector of standard inertial parameters and friction parameters to be identified, $\mathbf{\Phi} = [\mathbf{\Phi}_1^T ... \mathbf{\Phi}_{N_L}^T \ \mathbf{FC}^T \ \mathbf{FV}^T]^T$. For each segment i, 10 inertial parameters can be expressed in the joint frame $\mathbf{\Phi}_i = \begin{bmatrix} M_i & \mathbf{MS}_i^T & \mathbf{TI}_i^T \end{bmatrix}^T$, where M_i is the mass, $\mathbf{MS}_i = \begin{bmatrix} MSX_i & MSY_i & MSZ_i \end{bmatrix}^T$ is the 3-dimension vector of the first moment of inertia, and the 6-dimension vector $\mathbf{TI}_i = \begin{bmatrix} XX_i & YY_i & ZZ_i & XY_i & XZ_i & YZ_i \end{bmatrix}^T$ that gathers the components of the 3×3 tensor of inertia.

D. Inertial parameters identification

1) Base parameters identification: Eq. (3) can be used to identify $\mathbf{\Phi}$, the vector containing the standard inertial parameters. However, since $\mathbf{W}$ is not a full column rank matrix, a direct least squares approach is not suitable for its solution. This equation can be rewritten using the *so-called* base parameters (BP) as defined in [3] in a way that the regressor is of full column rank. Note that unless there is some coupling between joints, the friction parameters are always independent. Consequently, vector $\mathbf{\Phi}_b$ $(N_B \times 1)$ is the minimal identifiable set of inertial parameters required to describe the dynamics of the system. Since the BP are intrinsically related to the kinematic structure of the system they can be computed numerically [3]. Their computation consists in finding the equivalent regressor $\mathbf{W}_b$ $(N_J \times N_B)$ that is a full rank matrix by combining the linearly dependent columns. This results in the elimination and regrouping of the SIP into the vector $\mathbf{\Phi}_b$, and eq. (3) can be written as (see [3], [2]):

$$\mathbf{W}\mathbf{\Phi} = \mathbf{W}_b\mathbf{\Phi}_b = \mathbf{\Gamma} \tag{4}$$

Sampling (4) over a given motion, the identification problem for N_s time-samples becomes:

$$\begin{bmatrix} \mathbf{W}_b(1) \\ \vdots \\ \mathbf{W}_b(N_S) \end{bmatrix} \mathbf{\Phi}_b = \begin{bmatrix} \mathbf{\Gamma}(1) \\ \vdots \\ \mathbf{\Gamma}(N_S) \end{bmatrix} \tag{5}$$

$$\bar{\mathbf{W}}_b\mathbf{\Phi}_b = \bar{\mathbf{\Gamma}}$$

It can be solved by using a weighted Moore-Penrose pseudo-inverse matrix:

$$\mathbf{\Phi}_b^* = (\bar{\mathbf{W}}_b^T\mathbf{P}\bar{\mathbf{W}}_b)^{-1}\mathbf{P}\bar{\mathbf{W}}_b^T\bar{\mathbf{\Gamma}} \tag{6}$$

where $\mathbf{P}$ is a weight matrix based on the calculation of the relative standard deviation of the identified parameters [4]. The choice of an offline least-square identification process over an adaptive filter [9] to identify the inertial parameters has been made since it allows to obtain physically consistent inertial parameters. Moreover, adaptive filter convergence time to a stable estimate of an inertial parameters will be directly linked to the excitation motion resulting in the same overall estimation time [9] .

E. End-effector identification

The end-effector tool of a manipulator robot is more likely prone to modification. This will create dynamics but also geometric changes. In human, it has been shown that the shape of an handled object can be retrieved from the knowledge of its inertial parameter only [28]. Similarly, this paper proposes a novel method allowing to update the end-effector tool geometric parameters from its identified SIP using proprioceptive information.

1) Dynamics identification: A specific identification model was built to identify only the end-effector inertial parameters. It is based on two sets of grouped equations representing the trajectories without and with end-effector [29].

$$\begin{bmatrix} \bar{\mathbf{\Gamma}}^u \\ \bar{\mathbf{\Gamma}}^l \end{bmatrix} = \begin{bmatrix} \bar{\mathbf{W}}_b^u & 0 \\ \bar{\mathbf{W}}_b^l & \bar{\mathbf{W}}_L^l \end{bmatrix} \begin{bmatrix} \mathbf{\Phi}_b \\ \mathbf{\Phi}_L \end{bmatrix} \tag{7}$$

where upper and lower equations represent the trajectory without and with end-effector, respectively. $\bar{\mathbf{\Gamma}}^u$, $\bar{\mathbf{\Gamma}}^l$, $\bar{\mathbf{W}}_b^u$ and $\bar{\mathbf{W}}_L^u$ are the measured joint torques vectors and BP regressor matrices corresponding to the end-effector inertial parameters when the KLWR is unloaded and loaded, respectively. Note that for the last link the SIP and BP are equal. The link parameters $\mathbf{\Phi}_b$ and the end-effector inertial parameter $\mathbf{\Phi}_L$ are estimated by solving eq. (7) similarly to eq. (6).

2) Geometrical identification: The identification of the end-effector geometric parameters is based on the relation between inertial and geometric parameters. For example, a large size object will have large inertial parameters and a sharp shaped one will have moments of inertia around two axes larger than the moment of inertia about the remaining axis. Using this principle, it is possible to recognize the length and the width of a paint roller from a priori set look-up table. This look-up table contains the corresponding inertial and geometric parameters for each investigated painting tool.

From this look-up table, the smallest differences between identified and known parameters allow to determine which is the corresponding painting tool.

However, considering that several tools might be included in the look-up table, it is better to reduce the dimension of the vector containing the variables required to discriminate one tool among others. Therefore, the norm of the error of a lower dimensional space, created using a principal component analysis (PCA), of the inertial parameters was used. The

PCA was set by considering a set of N_T different tools. The SIP parameters (robot + tool) corresponding to the different tools are noted in the look-up table as $\mathbf{\Phi}_1, \ \cdots \mathbf{\Phi}_{N_T}$. The corresponding transformation matrices for converting to the N-dimensional PCA space are denoted as $\mathbf{U}_p \in \mathbb{R}^{10\times N}$. The reduced set of inertial parameters, i.e. in PCA space, $\mathbf{\Phi}_j^{pca} \in \mathbb{R}^N$ of the j^{th} tool can be expressed by the following equations:

$$\begin{aligned} \mathbf{\Phi}_j^{pca} &= \mathbf{U}_p^T \mathbf{\Phi} \\ &= \begin{bmatrix} \mathbf{U}_1 & \mathbf{U}_2 & \cdots & \mathbf{U}_N \end{bmatrix}^T \mathbf{\Phi}_j \\ &\text{with} \quad j = 1, \cdots, N_T \\ \bar{\mathbf{\Phi}} &= \begin{bmatrix} \mathbf{\Phi}_1 & \mathbf{\Phi}_2 & \cdots & \mathbf{\Phi}_{N_T} \end{bmatrix} \\ &= \mathbf{U}\mathbf{S}\mathbf{V}^T \\ &= \begin{bmatrix} \mathbf{U}_p & \mathbf{U}_{N+1} & \cdots & \mathbf{U}_{10} \end{bmatrix} \mathbf{S}\mathbf{V}^T \end{aligned} \tag{8}$$

where $\mathbf{U}$ is the unitary matrix from a singular value decomposition of $\bar{\mathbf{\Phi}}$ composed of all end-effector's SIP.
Thus, the error norm between the tool being identified $\mathbf{\Phi}_{Id}^{pca}$ and one from the look-up table can be calculated by $|| \ \mathbf{\Phi}_j^{pca} - \mathbf{\Phi}_{Id}^{pca} \ ||$ and $j = 1, \cdots, N_T$. Consequently, the tool with the smallest norm error in the PCA space will be selected.

III. Optimal exciting motions

A. B-spline trajectory parameterization

To solve the problem of generating exciting motions with an optimization, several approaches have been proposed to represent joint trajectories [6], [8], [10], [12], [15], [16]. The objective is to reduce the number of search variables, the computation time while having a complex trajectory and an accurate estimation of first and second order kinematics differentiation. In this paper, B-splines were retained to interpolate joint trajectories [8]. The principle of the joint parametrization is shown in Fig. 4. The joint trajectory lasts for a time T_F (with T_F being an integer in seconds) and is created from N_P way points which are equally spaced every 1 s. In the optimization, the joint angles ($\mathbf{q}(kT_S) \ k = 0, \cdots, N_S - 1$), velocities ($\dot{\mathbf{q}}(kT_S)$) and accelerations ($\ddot{\mathbf{q}}(kT_S)$) were interpolated at 100 Hz ($T_S = 0.01$ s). Also the trajectories were forced to have initial and final velocity and acceleration being zero thus fifth order B-splines were used. Finally, all joints trajectories were set to start and finish their motion at the same time.

B. Excitation criterion

As proposed by Jin et al. [10], three cost functions (condition number, Log determinant, and Hadamar inequality) were investigated to generate the optimal exciting motion [10]:

$$\begin{aligned} J_c &= \mathrm{cond}(\bar{\mathbf{W}}_\mathbf{b}) \\ J_d &= -\log(\det(\bar{\mathbf{W}}_\mathbf{b}^\mathbf{T} \bar{\mathbf{W}}_\mathbf{b})) \\ J_h &= -\log(\prod_{g=1}^{N_b} \sum_{k=1}^{N_J N_s} \mathbf{W}_{\mathbf{b}kg}^2) \end{aligned} \tag{9}$$

where $\mathrm{cond}(\mathbf{W}_\mathbf{b})$ is the condition number of the BP regressor matrix, $\mathbf{W}_{\mathbf{b}kg}$ is the k^{th} element of the g^{th} column of the regressor matrix $\mathbf{W}_\mathbf{b}$ and N_b is the number of BP.

C. Optimization process

The optimization problem that generates the constrained exciting motion can be formulated as:

$$\begin{aligned} \text{Find } \bar{\mathbf{q}}^* \in & \min_{\bar{\mathbf{q}} \in \mathbb{R}^{N_J \times N_s}} J_\# \\ \text{subject to} & \\ & q_j^- \leq \bar{q}_j \leq q_j^+ \\ & \dot{q}_j^- \leq \dot{\bar{q}}_j \leq \dot{q}_j^+ \\ & \ddot{q}_j^- \leq \ddot{\bar{q}}_j \leq \ddot{q}_j^+ \\ & \dot{q}_j(0) = \dot{q}_j(T_f) = 0 \\ & \ddot{q}_j(0) = \ddot{q}_j(T_f) = 0 \\ & \mid \Gamma_j \mid \leq \Gamma_j^+ \\ & \text{with} \quad j = 1, \cdots, N_J \\ & z_{ground} \leq \bar{z}_e, \bar{z}_w \\ & 0 \leq \bar{\mathbf{d}}_{vertex} \end{aligned} \tag{10}$$

where $J_\#$ is the cost function and $\# = c, d, h$. Joint angles, velocities, accelerations and torques must be within their physical limitations. q_j^-, q_j^+, $\dot{q}_j^-$, $\dot{q}_j^+$, $\ddot{q}_j^-$, $\dot{q}_j^+$, and Γ_j^+ are the lower and upper joint angle, velocity, acceleration and maximal torque limitations, respectively. Additionally in order to avoid auto-collision and collision with the environment, two kinematics constraints were added: the elbow and wrist frames must not collide with the ground and self-collisions must be avoided:

$$\begin{aligned} & z_{ground} \leq \bar{\mathbf{z}}_e, \bar{z}_w \\ & 0 \leq \bar{d}_{vertex} \end{aligned} \tag{11}$$

where $\bar{\mathbf{z}}_e$, $\bar{\mathbf{z}}_w$ and z_{ground} are position of elbow and wrist frame along ${}^G z$ axis and a virtual floor created to avoid collision with the actual ground. The constraints for auto-collision were simply defined using spheres attached to each link of the KLWR and by imposing the Euclidean distance $\bar{\mathbf{d}}_{vertex} \in \mathbb{R}^{12\times N_S}$, between two spheres to be always positive.

D. Determination of optimal motion duration time

The optimal exciting motion can be obtained by solving the problem defined in eq.10. However, there is no consensus in the literature on which cost function should be used to

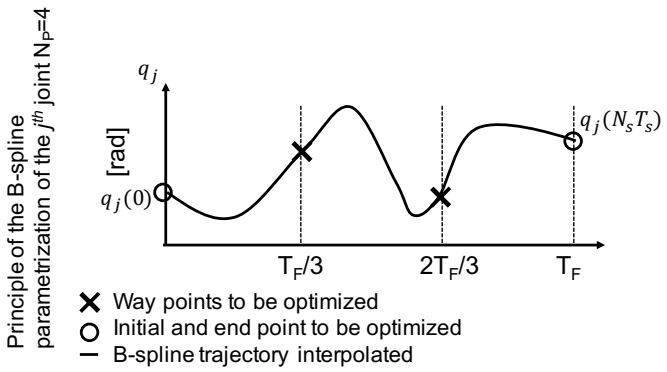

Fig. 4. B-spline trajectory via N_p points

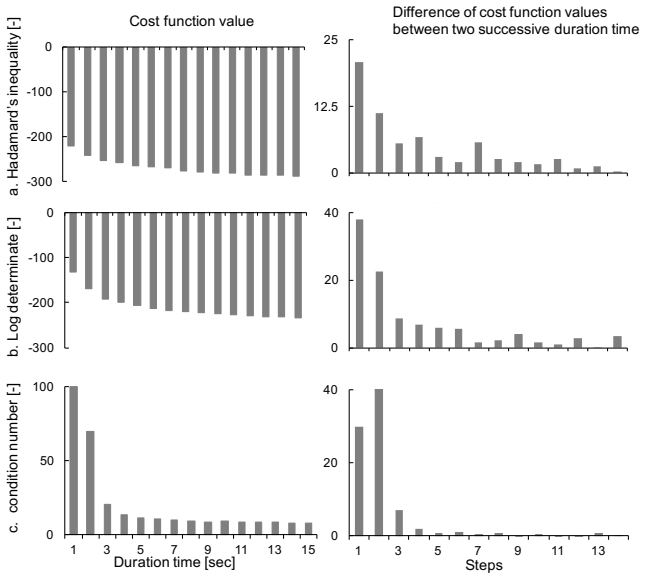

Fig. 5. (a) Relationships between cost values and duration time of the exciting motion, for each of the investigated cost function. (b) Difference of cost values between two successive duration time.

reach the best exciting motion in the shortest duration time. In order to determine the best duration time, the values of each criterion in function of the duration time T_F varying from 1 to 15 s were analyzed as represented in Fig. 5. On the right side of this figure, the differences of cost function values between two consecutive duration time are presented. From this figure, it is clear that no significant minimization of cost function values can be observed after 10 s. Also, we chose to have the same value for all three cost functions for comparison purpose. Consequently, the best trade-off between cost function minimization and time duration was set to 10 s.

E. Results of the dynamics identification of the KLWR

The performances of the three optimal trajectories were assessed experimentally. First, each of the three 10 s optimal exciting motions were played onto a KLWR and joint angles and torques were collected at 1 kHz. All data were low-pass filtered with a zero-phase lag filter (10 Hz , Butterworth 5^{th} order) and joint velocities and accelerations were obtained using a first order centred finite difference. Subsequently, BP were obtained for each of the three cost functions by solving eq. 6 with the corresponding experimental data. To assess the accuracy of the three identified models, the same cross validation motion of 20 s, visible in the accompanying video, was used for all three cases. The retained cross validation motion is of large amplitude, high dynamics and was not used in the identification process. Root Mean Square (RMS) and Normalized RMS (NRMS) differences between measured and estimated joint torques were calculated with this cross validation motion. The result of this analysis is shown in Fig. 6 for each joint. The average RMS difference between measured and estimated joint torques were: for J_c= 0.69 Nm, for J_d= 0.42 Nm and J_h= 0.45 Nm. Consequently, the exciting motions generated by the log determinant function J_d was

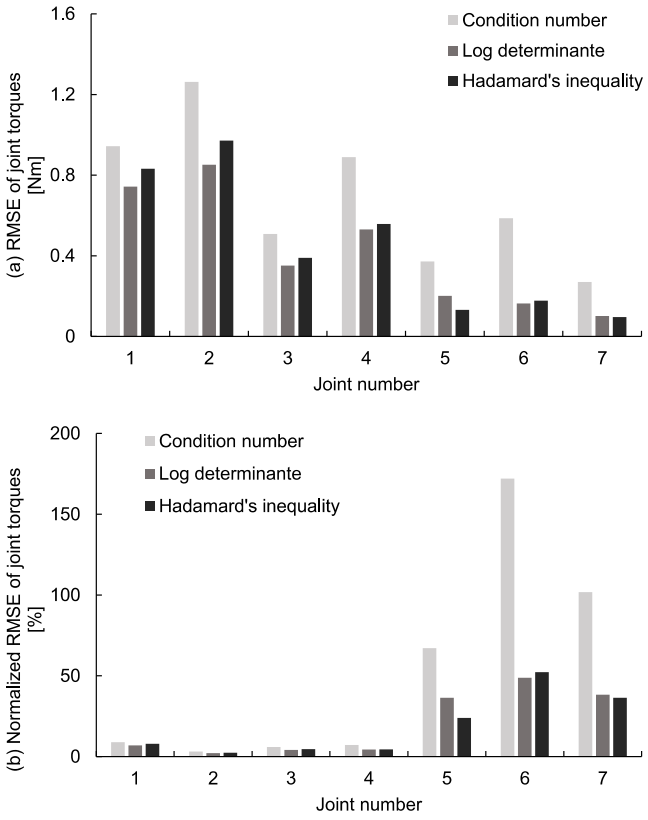

Fig. 6. (a) The root mean square errors and (b) normalized root mean square errors for estimated and measured joint torques for each 3 cost functions.

retained to identify the BP. As represented in Fig. 6(b) the highest NRMS was observed for the 6 th joint. This is expected since this joint does not carry a heavy load. Also a comparison between the identified, CAD data [24] and the BPs identified by Jubien et al. [5] is presented in table II. From this table the identified BP are in accordance to the ones proposed by Jubien et al.. As expected, differences can be observed since different robots were used. However, the reported standard deviation is lower in our case than in Jubien's paper. This shows the excellence of the proposed identification method.

IV. Motion planning

A. Cartesian trajectory generation

The Cartesian painting trajectory of the roller was obtained via a constrained optimization process. This optimization process aimed at generating a smooth painting trajectory, by minimizing the joint jerk, while handling KLWR's redundancy and taking into account the newly identified robot and end-effector inertial and geometric parameters to fully cover a designated surface. Moreover, this optimization aimed at minimizing the trajectory duration time T_C.

The Cartesian 6 DoF painting trajectory $\mathbf{P}_C = [\bar{P}_X \quad \bar{P}_Y \quad \bar{P}_Z \quad \bar{\theta}_X \quad \bar{\theta}_Y \quad \bar{\theta}_Z]^T$ was described by $\bar{\mathbf{P}}_{X,Y,Z}$ and by $\bar{\theta}_{X,Y,Z}$, the end-effector 3D positions and orientations

TABLE II
COMPARISON RESULTS BETWEEN THE IDENTIFIED BASE PARAMETERS IDENTIFIED, THE ONES PROPOSED BY JUBIEN ET AL. [5] AND THE ONES OBTAINED FROM CAD DATA.

	CAD		Identified		Jubien's	
Par.	$\mathbf{\Phi}$	$\%\sigma_{\Phi_r}$	$\mathbf{\Phi}$	$\%\sigma_{\Phi_r}$	$\mathbf{\Phi}$	$\%\sigma_{\Phi_r}$
XX_{2R}	1.32	-	1.35	0.30	1.30	1.5
ZZ_{2R}	1.32	-	1.36	0.34	1.28	1.6
MSY_{2R}	3.60	-	3.43	0.05	3.45	0.18
XX_{4R}	0.46	-	0.44	0.18	0.44	0.91
ZZ_{4R}	0.47	-	0.43	0.20	0.44	1.0
MSY_{4R}	-1.45	-	-1.34	0.05	-1.35	0.18
MSY_{5R}	0.036	-	0.047	0.86	0.040	3.6
MSY_{6R}	0.0104	-	0.034	0.50	0.035	6.4
MSY_7	0.0	-	0.001	13.3	0.006	14
FC_1	-	-	0.28	4.8	0.39	6.1
FC_2	-	-	0.43	4.1	0.52	5.5
FC_3	-	-	0.05	1.6	0.45	2.8
FC_4	-	-	0.16	5.8	0.32	3.7
FC_5	-	-	0.34	1.2	0.86	3.0
FC_7	-	-	0.20	1.2	0.08	6.0

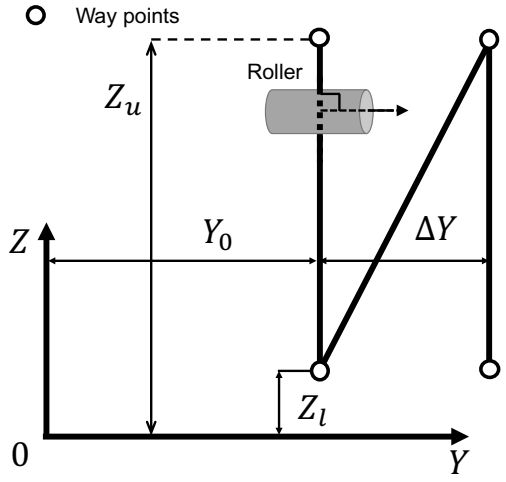

Fig. 7. Overview of the parameterization of Cartesian painting path

represented with Euler angles, respectively. The shape of the desired planar painting trajectory is described in Fig. 7, where Z_u and Z_l are the roller upper and lower extreme positions along the vertical axis, respectively. Y_0 is the initial horizontal roller position and ΔY is the horizontal distance travelled by the roller at each painting cycle. At each way point, defined by Z_u, Z_l, Y_0 and ΔY, both Cartesian speed and acceleration were defined to be null. The roller was also constrained to be perpendicular to the plane defined by the roller trajectory. To realize the desired Cartesian trajectory, the swivel angle φ, required in the calculation of the inverse geometric model (see section II.B), must be carefully selected. Indeed, its tuning is not unique and can lead to a discontinuous solution at some specific points along the trajectory. For these reasons, it was included as a search variable in the optimization process. Once the way points defined, the Cartesian trajectory was interpolated for each sample of time using a 5^{th} order B-splines. Finally, the path planning optimization problem boils down to find $\mathbf{x}_{opt} = [T_C \ \varphi \ Z_u \ Z_l \ Y_0 \ \Delta Y] \in \mathbb{R}^6$ that solves the following problem:

$$
\begin{aligned}
\text{Find } \mathbf{x}^*_{opt} \in \ & \min_{\mathbf{x}_{opt}\in\mathbb{R}^6} T_C + \sum_{j=1}^{N_J}\sum_{k=1}^{N_S} \dddot{q}_{jk}^{igm\,2} + \frac{1}{(Z_u - Z_l)\Delta Y} \\
\text{subject to} \\
& q_j^- \le \bar{q}_j^{igm} \le q_j^+ \\
& \dot{q}_j^- \le \dot{\bar{q}}_j^{igm} \le \dot{q}_j^+ \\
& \ddot{q}_j^- \le \ddot{\bar{q}}_j^{igm} \le \ddot{q}_j^+ \\
& \mid \Gamma_j \mid = \Gamma_j^+ \\
& \text{with} \quad j = 1, \cdots, N_J \\
& Z^- \le Z_u, \ Z_l \le Z^+ \\
& Z_l \le Z_u \\
& Y^- \le Y_0 \le Y^+ \\
& Y^- \le Y_0 + N_r \Delta Y \le Y^+ \\
& \Delta T \le w_L
\end{aligned}
\tag{12}
$$

where $\bar{\mathbf{q}}^{igm}$ is the joint trajectory calculated from the inverse geometric model, Z^-, Z^+, Y^- and Y^+ are the upper and lower roller position along the vertical and horizontal axes, respectively. w_L is the paint roller width coming from the identification process, and N_r is the number of times the roller returns to the maximum vertical position Z_u. The last constraint ensure that there are no unpainted parts.

To summarize, this optimization problem minimizes an hybrid cost function composed of the duration time, the norm of the joint jerks and maximize the painting area while ensuring dynamics and kinematics feasibility.

V. POSITION AND FORCE CONTROL LAW

To follow the optimally designed Cartesian trajectory the position and force Cartesian controller, presented in Fig, 8 was implemented.

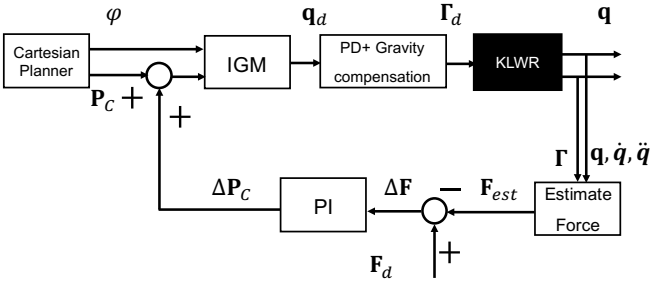

Fig. 8. Position and force control scheme retained for the investigated painting task.

A. Joint controller

A classical joint space PD controller with gravity compensation was implemented [30]. Since the dynamics models of the robot and of the painting tool were already identified, the PD control can be expressed as:

$$
\mathbf{\Gamma}_d = \mathbf{K}_p(\mathbf{q}_d - \mathbf{q}) + \mathbf{K}_d(\dot{\mathbf{q}}_d - \dot{\mathbf{q}}) + \hat{\mathbf{G}}(\mathbf{q}) \tag{13}
$$

where $\mathbf{K}_p$ and $\mathbf{K}_d$ are $(N_J \times N_J)$ diagonal matrices for proportional and derivative gains tuned experimentally. $\mathbf{q}_d$ $(N_J \times 1)$ and $\mathbf{q}$ $(N_J \times 1)$ are the vectors of desired and measured joint angles, respectively. $\dot{\mathbf{q}}_d$ and $\dot{\mathbf{q}}$ are obtained by first order backward difference with respect to $\mathbf{q}_d$ and $\mathbf{q}$. $\hat{\mathbf{G}}(\mathbf{q})$ $(N_J \times 1)$ is the vector of gravitational terms computed from the identified inertial parameters.

B. External force estimation

Thanks to the excellent identification of the KWLR and of its end-effector, the external forces can be estimated from the measured joint torques and the following equations [21]:

$$\begin{aligned} \boldsymbol{\Gamma} &= \hat{\mathbf{M}}(\mathbf{q})\ddot{\mathbf{q}} + \hat{\mathbf{C}}(\mathbf{q}, \dot{\mathbf{q}}) + \hat{\mathbf{G}}(\mathbf{q}) + \boldsymbol{\Gamma}_{ext} \\ &= \boldsymbol{\Gamma}_{dyn} + \boldsymbol{\Gamma}_f + \boldsymbol{\Gamma}_{ext} \\ \mathbf{F}_{est} &= (\mathbf{J}^T)^{+}\boldsymbol{\Gamma}_{ext} \\ &= (\mathbf{J}^T)^{+}(\boldsymbol{\Gamma} - \boldsymbol{\Gamma}_{dyn}) \end{aligned} \tag{14}$$

where $\mathbf{J}$ is $(6 \times N_J)$ robot Jacobian matrix. $\hat{\mathbf{M}}(\mathbf{q})$ $(N_J \times N_J)$ is the identified robot inertia matrix, $\hat{\mathbf{C}}(\mathbf{q}, \dot{\mathbf{q}})$ $(N_J \times 1)$ is the vector containing the identified Coriolis and centrifugal terms. $\boldsymbol{\Gamma}$ and $\boldsymbol{\Gamma}_{dyn}$ are the measured and estimated joint torques, respectively. $\mathbf{F}_{est}$ (6×1) is the estimated vector of the external forces in Cartesian space.

C. Force control

The proposed control scheme is composed of two embedded control loops [31]. The outer loop controls the external forces and the inner one controls the Cartesian end-effector's pose (Fig. 8). The additional displacement due to the force control to the desired Cartesian 3D position is given by:

$$\Delta\mathbf{P}_c = \mathbf{K}_p^f(\mathbf{F}_d - \mathbf{F}_{est}) + \mathbf{K}_i^f \int_{T_0}^{T} (\mathbf{F}_d - \mathbf{F}_{est}) \tag{15}$$

where $\Delta\mathbf{P}_c$ is the additional displacement reference signal in Cartesian space, $\mathbf{F}_d$ is desired external force and $\mathbf{K}_p^f$, $\mathbf{K}_i^f$ are the proportional and the integral gains, respectively.

VI. Experimental Validation

In order to validate the proposed approach, a large and a small paint rollers were used. The length, width and weight of the large one were 0.35 m, 0.2 m and 0.2 kg respectively. The length and width of the small one were 0.33 m and 0.10 m. Its weight was 0.1 kg. In order to feed the paint roller look-up tables, dynamics identification experiments with both tools were performed. The corresponding geometric and inertial parameters of each tool were associated.

A. Paint roller identification result

Table III presents the values of identified inertial parameters for both paint rollers. It can be seen that the two identified masses are closed to their reference values. Fig. 10 shows a comparison of the measured and estimated joint torques during a trajectory used for the identification of the large roller. T The sixth first joint torques were very well estimated while the last one displays more difference. This is due to the fact that the tool CoM is very close on the z-axis of the joint 7 and that the torque due to the inertial parameters is much smaller than the one due to friction. Nevertheless, the amplitude of this signal was very small, inferior to 0.5 Nm.

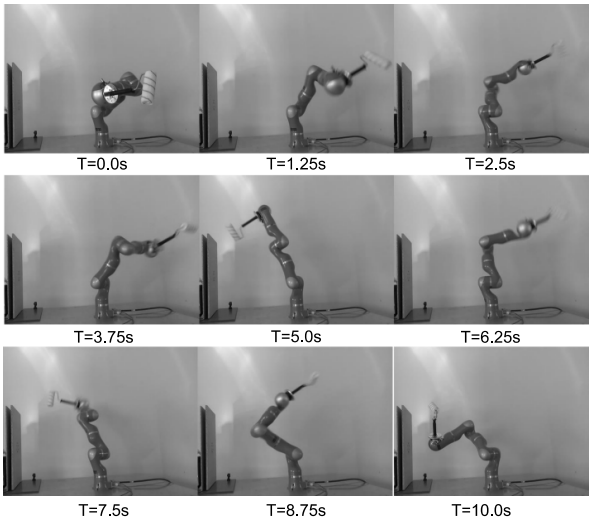

Fig. 9. Optimal exciting motion of 10 s used to identify the inertial BP. the trajectory was generated by minimizing the log determinant criterion. The complete trajectory is visible in the accompanying video and provided in supplementary material.

TABLE III
IDENTIFIED INERTIAL PARAMETERS FOR BOTH PAINT ROLLERS.

	Large roller		Small roller	
Par.	$\boldsymbol{\Phi}$	$\%\sigma_{\Phi_r}$	$\boldsymbol{\Phi}$	$\%\sigma_{\Phi_r}$
M [kg]	2.37×10^{-1}	0.5	9.73e-2	1.3
MSX [kgm]	-3.93×10^{-3}	8.1	4.54×10^{-5}	28.4
MSY [kgm]	-1.53×10^{-5}	21.0	7.17×10^{-5}	25.4
MSZ [kgm]	6.50×10^{-2}	0.6	2.44×10^{-2}	1.4
XX [kgm^2]	1.98×10^{-2}	1.9	7.36×10^{-3}	4.4
YY [kgm^2]	2.10×10^{-2}	2.0	7.12×10^{-3}	5.1
ZZ [kgm^2]	2.08×10^{-3}	14.9	1.55×10^{-4}	31.0
XY [kgm^2]	5.57×10^{-4}	56.6	2.01×10^{-4}	102.8
XZ [kgm^2]	6.27×10^{-4}	41.5	-4.25×10^{-4}	54.7
YZ [kgm^2]	8.25×10^{-5}	49.9	2.06×10^{-4}	47.5

The lengths and widths of both paint rollers were determined by sorting the norm errors between identified inertial parameters in the PCA space and the results contained in the look-up table. The PCA was able to reduce the search space from 10 variables to a 4 dimensions problem. This is encouraging for future use of this method with more paint rollers.

B. Position and Force control experiment

The position and force control experiment was performed using the proposed controller and identified models. Fig. 11 presents the experimental environment. On a custom painting wall (height: 0.8 m, width: 0.6 m), a global coordinate system made to coincide the x-axis with the robot's push, i.e. normal, direction, the y-axis with the horizontal direction and the z-axis with the vertical direction. The center of the wall was

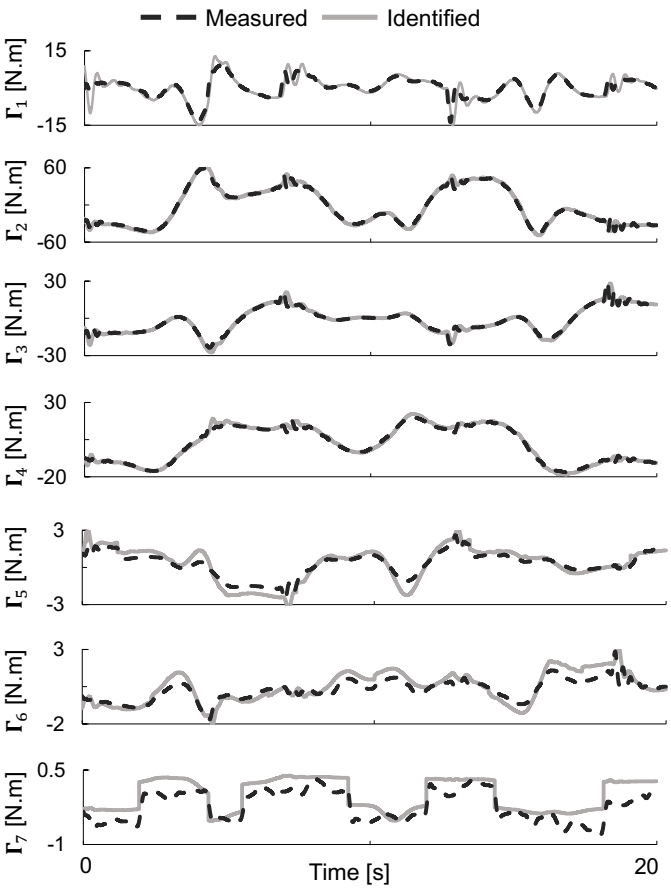

Fig. 10. Comparison of the measured and estimated joint torques from identification

located at x:-0.8 m, y:0.3 m and z:0.4 m. A six axes force sensor (ATI, Mini45), used to measure reference forces data, was located in the center of the wall. The desired external forces were set to $\mathbf{F}_d = (-30, 0, 0)$ N.

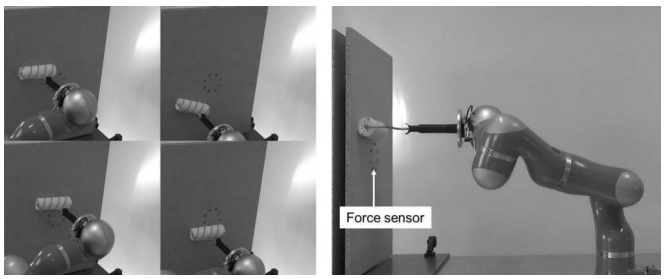

Fig. 11. Snapshot showing the experimental setup and the painting experiment. The complete experimentation is visible in the accompanying video.

Fig. 12 presents the desired painting trajectory generated by the optimization process 12 and using the identified models in both roller cases. The duration time of each trajectory were 50 s and 46 s for large roller and for small roller cases, respectively.

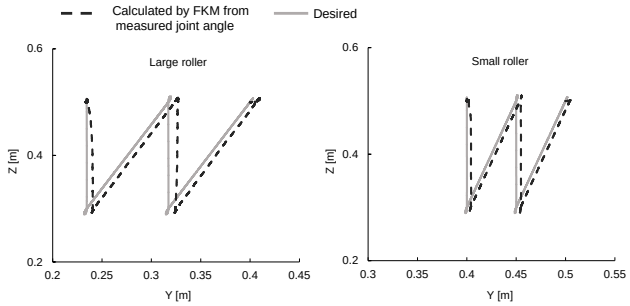

Fig. 12. Comparison between the desired and actual experimental planar trajectories performed in contact with the wall.

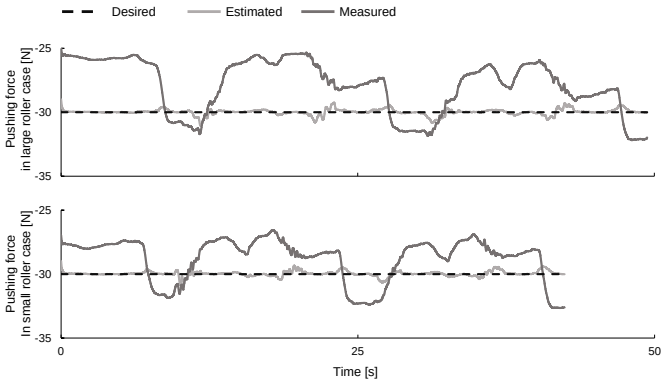

Fig. 13. Representative results showing the desired normal external force, the estimation from the proposed method and the one measured by an external force sensor.

Fig. 13 presents the desired, estimated and measured external forces between end-effector and the painting wall in the case of the large paint roller. Two cases are displayed. In Fig. 13a, the estimated external force is used in the control feedback. In Fig. 13b the force sensor measurements are used in the control feedback. The corresponding RMS and NRMS differences are given in the Table IV. From these results, it can be stated that the proposed control system can accurately estimate and control the external forces.

TABLE IV
ACCURACY ASSESSMENT OF THE NORMAL EXTERNAL FORCE ESTIMATE.

	Large roller		Small roller	
	RMS	NRMS	RMS	NRMS
Estimated/Measured	2.9 N	9.8 %	2.0	6.8 %
Estimated/Desired	0.2 N	0.7 %	0.2	0.7 %
Measured/Desired	2.9 N	10.5 %	2.0	7.0 %

VII. CONCLUSION

In this paper, a novel method for the fast identification of inertial parameters, of end-effector geometrics parameters and a force control framework applied to the popular KLWR have been developed. This paper shows the benefit of identifying a

serial robot with a real dynamic application. During a roller painting task, using a classical model based approach [20], [21] and thanks to the excellent model identification it was possible to estimate the external forces without a force sensor mounted at the end-effector. The results are in line with the relevant literature [14], [21] even if the investigated task are of different nature. To perform the identification data collected over an exciting motion of 10 s were used. It was generated by an optimization process minimizing $\log\{\det(\cdot)\}$ cost function, and by chosing the best trade-off between duration time and excitation level. Other fields [35] have proposed other cost functions such as the log(cond()) that could be investigated in the future. The use of Log is of a great interest to normalize the condition number for badly conditioned system. Also the proposed framework is able to recognize the geometric parameters from identified BSIP using a PCA and a look-up table. The current experiment includes only two types of end-effectors, but the use of PCA reduction space is very interesting for real industrial applications involving numerous type of painting tools. Moreover, the PCA could be used to interpolate geometric parameters in a reduced space in the case of unknown tool. Future works will consist in extending this method to much more painting tools including length variables rollers and brushes. By identifying both dynamic and geometric models, similarly to Wilson et al. [11], a painting trajectory satisfying dynamic robot limitations could be generated from the updated models. Because the current end-effectors were of small weights the painting trajectories were very similar. However, the use of the proposed method will be crucial in case of a heavy payload. Nevertheless, the painting trajectory was executed using a classical position/force controller presented in Fig 8. In the future, we plan to improve the proposed identification method by providing statistical bounds to estimated parameters. It could be beneficial to more advance inverse dynamics controllers [18] by reducing the conservatism in the design and improving the overall efficiency of the controller. From the results shown in Fig. 13, it was found that this controller can control the estimated external force satisfactorily using the feedback of external forces estimated without force sensor (RMS error inferior to 3 N).

ACKNOWLEDGMENT

This study was supported by the Japan Society for Promotion of Science (No PE14768).

REFERENCES

[1] M. H. Raibert, J. J. Craig, "Hybrid position/force control of manipulators," *ASME J. of Dynamic Systems, Measurement, and Control*, vol. 103, pp. 126-133, 1981.

[2] M. Gautier, W. Khalil, "On the identification of inertial parameters of robots," *IEEE Int. Conf. on Decision Control*, pp. 2264-2269, 1998.

[3] W. Khalil, E. Dombre, "Identification of the dynamic parameters," in *Modeling, identification and control of robots*, 1st ed. Butter-worth-Heinemann, UK, pp. 291-311, 2002.

[4] M. Gautier, G. Venture, "Identification of standard dynamic parameters of robots with positive definite inertia matrix," *IEEE/RSJ Int. Conf. on Int. Robots and Systems*, pp. 5815-5820, 2013.

[5] A. Jubien, M. Gautier, A. Janot, "Dynamic identification of the Kuka LWR robot using motor torques and joint torque sensors data," *Proc. IFAC* vol. 47, pp. 8391-8396, 2014.

[6] W. He, W. Ge, Y. Li, Y. Liu, C. Yang, C. Sun ,"Model Identification and Control Design for a Humanoid Robot," *IEEE Transactions on Systems, Man, and Cybernetics Systems* , pp. 1-13, 2016.

[7] C. Gaz, F. Flacco, and A. De Luca, Identifying the dynamic model used by the KUKA LWR: A reverse engineering approach, *IEEE Int. Conf. on Robot. Autom.*, pp. 13861392, 2014.

[8] V. Bonnet, P. Fraisse, A. Crosnier, M. Gautier, G. Venture, "Optimal exciting dance for identifying inertial parameters of an anthropomorphic structure,"*IEEE Tran. Robotics*, pp. 823-836, 2016

[9] V. Joukov, V. Bonnet, G. Venture, D. Kulic, "Constrained dynamic parameter estimation using the extended Kalman filter," *IEEE/RSJ Int. Conf. on Int. Robots and Systems*, pp. 3654-369, 2015.

[10] J.Jin and N.Gans, "Parameter identification for industrial robots with a fast and robust trajectory design approach," *Elsevier J. of Robotics and Computer-Integrated Manufacturing*, vol. 31, pp. 21-29, 2015.

[11] A.D. Wilson, J.A. Schultz, A.R. Ansari, T.D. Murphey, "Dynamic task execution using active parameter identification with the Baxter research robot," *IEEE Tran. Autom. Sc. Eng.,*, pp. 391-397, 2017.

[12] G.A. Fontanelli, F. Ficuciello, L. Villani, B. Siciliano, "Modelling and identification of the da Vinci Research Kit robotic arms,"*IEEE/RSJ Int. Conf. on Int. Robots and Systems*, pp. 2017.

[13] A. Colome, D. Pardo, G. Alenya, C. Torras, "External Force Estimation During Compliant Robot Manipulation,"*IEEE Int. Conf. on Robot. Autom.*, pp. 2298-2304, 2015.

[14] A. Wahrburg, E. Morara, G. Cesari, B. Matthias, H. Ding, "Cartesian contact force estimation for robotic manipulators using Kalman filters and the generalized momentum", *IEEE Int. Conf. Automation Science Eng.*, pp. 1230-1235, 2015.

[15] J. Swevers, C. Ganseman, D. B. Tükel and J. D. Schutter, "Optimal robot excitation and identification," *IEEE Trans. on Robot. Autom.*, vol. 13, pp. 730-740, 1997.

[16] W. Rackl, R. Lampariello, G. Hirzinger, "Robot excitation trajectories for dynamic parameter estimation using optimized B-Splines," *IEEE Int. Conf. on Robot. Autom.*, pp. 2042-2047, 2012.

[17] A. Wahrburg and S. Zeiss and B. Matthias and H. Ding, "Contact force estimation for robotic assembly using motor torques," *2014 IEEE Int. Conf. on Automation Science and Engineering (CASE)*,pp. 1252-1257, 2014.

[18] A. Del Prete, N. Mansard, "Robustness to joint-torque-tracking errors in task-space inverse dynamics,"*IEEE Tran. Robotics*, pp. 1091-1105, 2016.

[19] T.H. Pham, S. Caron, A. Kheddar, "Multi-Contact Interaction Force Sensing from Whole-Body Motion Capture," *IEEE Tran. Industrial Informatics*, to appear. 2017.

[20] Magrini, F. Flacco, A. De Luca, "Control of Generalized Contact Motion and Force in Physical Human-Robot Interaction," *IEEE Int. Conf. on Robot. Autom.*, pp. 2298-2304, 2015.

[21] F. Flacco, and A. De Luca, Estimation of contact forces using a virtual force sensor, *IEEE/RSJ Int. Conf. on Intelligent Robots Systems*, pp. 21262133, 2014.

[22] E. d. Sol, R. King, R. Scott and M. Ferre, "External force estimation for teleoperation based on proprioceptive sensors," *SAGE J. of Advanced Robotic Systems*, DOI: 10.5772/58468, 2014.

[23] Link to the optimal trajectories and identification pipeline. https://www.dropbox.com/sh/0p7sg0w1f6dc9bf/AADm_uLhyA8Cet1ymOlXidGBa?dl=0

[24] M. Cefalo, "Notes on the Kuka LWR4 dynamic model," Available Online.

[25] Y. Fujimoto, S. Obata, A. Kawamura, "Robust biped walking with active interaction control between foot and ground," *IEEE Int. Conf. on Robot. Autom.*, pp. 2030-2035, 1998.

[26] D. Tolani, A. Goswami and N. Badler, "Real-time inverse kinematics techniques for anthropomorphic limbs," *Elsevier J. of Graphical Models*, vol. 62, pp. 353-388, 2000.

[27] W. Khalil, D. Creusot, "SYMORO+: A system for the symbolic modeling of robots," *Cambridge J. of Robotica*, vol. 15, pp. 153-161, 1997.

[28] M. T. Turvey, "Dynamic Touch," *Science Watch J. of American Psychologist* vol. 51, pp. 1134-1152, 1996.

[29] W. Khalil, M. Gautier and P. Lemoine, "Identification of the payload inertial parameters of industrial manipulators," *IEEE Int. Conf. on Robot. Autom.*, pp. 4943-4948, 2007.

[30] A. De Luca, B. Siciliano, L. Zollo "PD control with on-line gravity compensation for robots with elastic joints: Theory and experiments," *Elsevier J. of Automatica*, vol. 41, no. 10, pp. 1809-1819, 2005.

[31] J. D. Schutter, H. V. Brussel, "Compliant robot motion II. A control approach based on external control loops," *SAGE J. of Robotics Research*, vol. 7, pp. 18-33, 1988.

[32] K.S. Eom, I.H. Suh, W.K. Chung, and S.R. Oh. "Disturbance observer based force control of robot manipulator without force sensor," *IEEE Int. Conf. on Robot. Autom.*, pp. 3012-3017, 1998.

[33] A. Alcocer, A. Robertsson, A. Valera, and R. Johansson. "Force estimation and control in robot manipulators," *IFAC Symp. on Robot Control*, pp. 31-36, 2003.

[34] M. Linederoth, A. Stolt, A. Robertsson, R. Johansson, "Robotic force estimation using motor torques and modeling of low velocity friction disturbances," *IEEE/RSJ Int. Conf. on Int. Robots and Systems*, pp. 3550-3556, 2013.

[35] S. Jahandari, A. Kalhor, B.N. Araabi, "Online Forecasting of Synchronous Time Series Based on Evolving Linear Models", *IEEE Tran. Sys., Man, and Cybernetics: Systems*, in-press, 2018.